Control-Free Inductive-Power-Transfer Transmitter with Misalignment Tolerance

Hai Xu, Zhicong Huang, *Senior Member, IEEE*, Xiaolu Lucia Li, *Member, IEEE*, and Chi K. Tse, *Fellow, IEEE*

***Abstract*—Misalignment tolerance is a critical and challenging requirement for inductive power transfer (IPT) systems. To address this challenge, a transmitter (Tx) pad combining unipolar and bipolar coils is employed. This hybrid design enhances the magnetic flux, allowing a unipolar (or bipolar) receiver (Rx) pad to effectively capture it even in misaligned conditions. However, it is important to note that misalignment in positive and negative directions leads to a non-axially symmetric magnetic field distribution, resulting in a polarity reversal of the mutual inductance. This often requires complex detection and active control mechanisms to ensure misalignment tolerance, which can negatively impact system robustness. To overcome this challenge, this paper introduces a control-free and misalignment-tolerant IPT system. The proposed system utilizes a hybrid Tx pad consisting of rectangular and solenoidal coils, while the Rx pad is a rectangular coil. In order to eliminate the need for detection and control, a novel excitation method for the Tx coils is proposed, along with comprehensive schematics, modeling, and analysis. Additionally, the paper provides detailed parameter design considerations to minimize output fluctuation and achieve soft switching. Notably, the system maintains high power efficiency across the entire range of misalignment. To validate the effectiveness of the proposed control-free IPT system with misalignment tolerance, a 1-kW experimental prototype has been constructed. The experimental results show that the output voltage is 150 V with less than 4% fluctuation and the efficiency can be maintained at 90% with variation below 0.8% over a misalignment of 50% of the RSP length.**

***Index Terms*—Inductive power transfer, misalignment tolerance, control-free, complementary.**

I. Introduction

INDUCTIVE power transfer (IPT) technology has emerged as an attractive solution, enabling wireless power transfer through magnetic coupling without physical contact [1]–[4]. IPT is a promising alternative for EV charging due to its user-friendly and maintenance-free operations [5]–[8]. However, without misalignment tolerance, IPT systems can only function optimally when the receiver (Rx) pad is precisely aligned with the transmitter (Tx) pad. This precise positioning system is often unavailable in practical IPT applications, making the design for misalignment tolerance crucial [9].

To achieve misalignment tolerance, one effective approach is to adopt an asymmetric design that ensures a nearly uniform magnetic flux distribution [10]–[13]. For instance, multi-identical coils wound overlap with each other is introduced, such as the configuration proposed in Refs. [10], [11]. This can also be accomplished by using a transmitter (Tx) pad with an area several times larger than that of the corresponding receiver (Rx) pad. Previous studies have explored the use of multiple rectangular coils configured into a Tx planar structure to generate a nearly uniform magnetic field. This design allows the Rx pad to be displaced within the Tx planar without causing significant power fluctuations [12], [13]. However, it is important to note that implementing the Tx planar design introduces complexities in terms of the drive circuit and control scheme. These complexities arise from the need to precisely activate individual Tx pads and suppress circulating currents among them. To simplify control, hybrid compensation-based schemes have been developed to achieve complementary output gains [14]–[17]. Typically, the IPT system employs two compensation topologies, each with a resonant tank that exhibits contrasting output characteristics. One resonant tank increases output with misalignment, while the other demonstrates the opposite behavior. By complementing the output variations of these two resonant tanks, the overall output can effectively disregard misalignment. For instance, the S-S and LCC-LCC compensation networks, featuring different connection styles (input-parallel-output-parallel and input-series-output-series configurations), have been proposed to maintain nearly constant output current over a range of misalignment [14], [15]. Similarly, the LCC-S and S-LCC compensation networks, with input-parallel-output-series connection style, are utilized to achieve misalignment-tolerant voltage output [18]. The misalignment tolerance achieved through these hybrid compensation schemes relies on complementary transfer gains provided by the two compensation circuits, rather than maintaining consistent magnetic flux despite misalignment. Another gain-based design method utilizing the detuned design principle has also been introduced for pad misalignment tolerance [19], [20]. However, the output characteristics (e.g., output voltage or output current) of IPT systems with detuned design are load-dependent. In addition, a significant concern with these hybrid compensation-based schemes and detuned design schemes is that the magnetic flux decreases as misalignment increases, leading to noticeable efficiency degradation. This phenomenon is evident in the

Manuscript received 26 December 2024, revised 18 February 2025, accepted 6 April 2025. This work is supported by the Science and Technology Planning Project of Guangdong Province under Grants 2023A0505050124 and 2023B0909050007, the Natural Science Foundation of Guangdong Province under Grant 2023A1515011623, the Guangzhou Municipal Science and Technology Bureau under Grant 2025A04J7064, and Hong Kong RGC Theme-Based Research Scheme Project T23-701/20R. (Corresponding author: Zhicong Huang)

Hai Xu and Zhicong Huang are with the Shien-Ming Wu School of Intelligent Engineering, South China University of Technology, Guangzhou, 510006, China (e-mail: wixuh@mail.scut.edu.cn, zhiconghuang@scut.edu.cn).

Xiaolu Lucia Li is with the School of Integrated Circuits, Sun Yat-sen University, China (email: lixlu8@mail.sysu.edu.cn).

Chi K. Tse is with the Department of Electrical Engineering, City University of Hong Kong, Hong Kong, China (email: cktse@ieee.org)

Digital Object Identifier TXXXxxxx.0000.0000.0000

experimental results presented in the aforementioned work.

An alternative approach to achieving misalignment tolerance focuses on maintaining a consistent magnetic flux despite misalignment [21]–[25]. This approach involves connecting two transmitter (Tx) coils in an anti-series configuration (i.e., a Litz wire is wound into two coils, one coil being counterclockwise and the other clockwise.) to ensure that their magnetic couplings remain consistently different regardless of the misalignment. Chen *et al.* [23] implemented this design concept by using an anti-series configuration of a rectangular coil and a circular coil on the Tx pad, which maintains a nearly constant mutual inductance difference aligned with the pad misalignment. Additionally, Zhang *et al.* [24] proposed the use of four rectangular coils in an inverse series configuration on the Tx side to compensate for misalignment. Through the anti-series connection, the variations cancel out, allowing for a consistent magnetic field even in the presence of misalignment. However, it is important to note that this magnetic field cancellation may weaken the power transfer capacity and require increased copper usage for constructing the magnetic pad. Furthermore, the layout of multiple anti-series coils on the same side introduces challenges related to cross coupling, making the design of anti-series coils complex [24].

Instead of relying on magnetic field cancellation, a hybrid design of unipolar and bipolar coils can be employed to maintain consistent magnetic flux in the presence of misalignment, utilizing the concept of complementary magnetic flux [26], [27]. The unipolar and bipolar coils generate vertical and horizontal magnetic fluxes that exhibit inverse trends with misalignment. By combining these fluxes, a consistent overall magnetic flux can be achieved. One well-known example of a hybrid unipolar and bipolar magnetic pad is the double-D quadrature pad (DDQP). It consists of a rectangular coil in quadrature with a double-D coil. The magnetic fluxes generated by the unipolar and bipolar coils depend on their excitation currents. Typically, when subjected to identical excitation currents, the bipolar coil exhibits a centric axially symmetric magnetic field distribution in both negative and positive misalignment directions, while the unipolar coil has an axially symmetric distribution. However, achieving complementary characteristics in the overall magnetic flux throughout the entire misalignment range presents a challenge. This challenge will be discussed further in Section II. To achieve misalignment tolerance, the unipolar and bipolar coils are always set on the Rx side and connected with the individual rectifier bridge in series or parallel [28], [29]. However, this results in a complex and cumbersome receiver side that demands more installation space, making it less practical for real-world applications [30], [31]. To simplify the Rx side, the hybrid pad is configured as the Tx pad. In this way, complex detection and active control mechanisms are required for the output. In the work proposed by Jo *et al.* [32], the unipolar and bipolar coils are independently driven, and three operating modes are utilized (unipolar coil only, bipolar coil only, and both coils) based on the misalignment conditions. Real-time detection of the coupling coefficient is necessary to determine the appropriate operating mode.

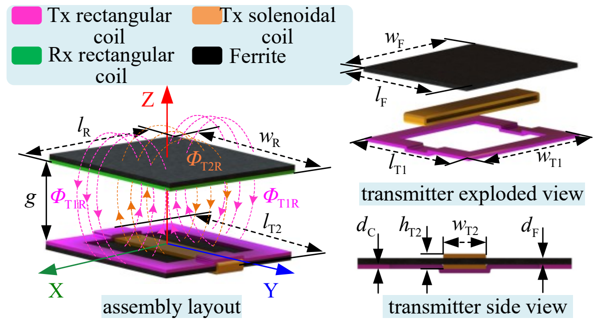

Fig. 1. Proposed rectangular-solenoidal pad coupler (RSP-RP).

TABLE I
PARAMETERS OF THE COUPLER

Symbols	Parameters	Value
l_{R}	Length of Rx rectangular coil	300 mm
w_{R}	Width of Rx rectangular coil	300 mm
l_{T1}	Length of Tx rectangular coil	300 mm
w_{T1}	Width of Tx rectangular coil	300 mm
l_{T2}	Length of Tx solenoidal coil	306 mm
h_{T2}	Height of Tx solenoidal coil	9 mm
w_{T2}	Width of Tx solenoidal coil	27 mm
l_{F}, w_{F}	Ferrite dimensions	300 mm, 300 mm
d_{F}		3 mm
d_{C}	Diameter of Litz wire	3 mm
g	Air gap distance	60 mm
N_{T1}	Turn number of Tx rectangular coil	10
N_{T2}	Turn number of Tx solenoidal coil	9
N_{R}	Turn number of Rx rectangular coil	10
P_{N}	Turn space of coils	0mm

This paper introduces a control-free and misalignment-tolerant IPT system as an alternative to traditional detection and control methods. The IPT system comprises a hybrid transmitter (Tx) pad consisting of rectangular and solenoidal coils, as well as a receiver (Rx) pad equipped with rectangular coils. The paper presents a novel excitation method for the Tx coils, supported by comprehensive schematics, modeling, and analysis. This approach enables misalignment tolerance without the need for detection and control mechanisms. Furthermore, the paper outlines the parameter design process to minimize output fluctuation and ensure smooth switching throughout a wide range of misalignment. Apart from maintaining a nearly constant output voltage, the proposed system also boasts high power efficiency due to the consistent magnetic flux across the entire misalignment range. The proposed scheme is validated through a 1-kW experimental prototype. The novelties and contributions of this paper are summarized as follows.

1) This paper proposes a control-free and misalignment-tolerant IPT system as an alternative to traditional detection and control methods. The system incorporates the concept of power transfer efficiency misalignment tolerance based on the magnetic flux complementary principle. The proposed IPT system is designed to accommodate a hybrid transmitter pad comprising unipolar and bipolar coils, as well as a receiver pad equipped with a unipolar (or bipolar) coil.
2) A novel excitation method for the hybrid transmitter pad consisting of unipolar and bipolar coils is presented, supported by detailed schematics, modeling, and analy-

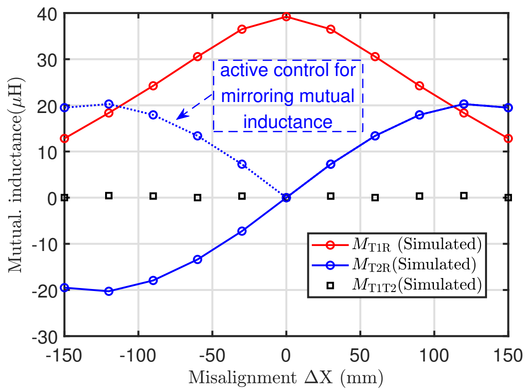

Fig. 2. Mutual inductances of RSP-RP versus misalignments along X-axis.

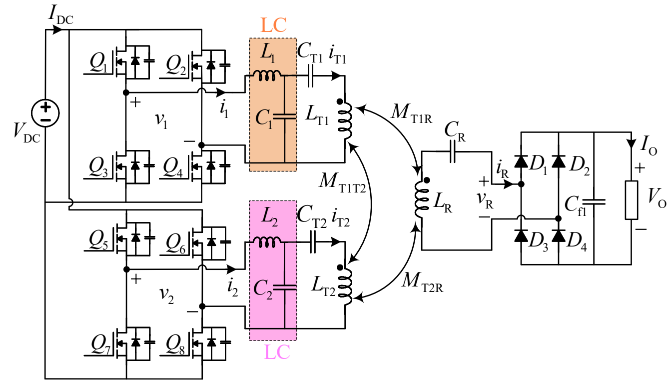

Fig. 3. Proposed IPT charging system with RSP-RP coupler.

sis. This approach enables the proposed IPT to operate regardless of the mutual inductance polarity and achieves misalignment tolerance without the need for detection and control mechanisms.

3) The paper outlines the parameter design process to minimize output fluctuation and ensure smooth soft switching throughout a wide range of misalignment. Apart from maintaining a nearly constant output voltage, the proposed system also boasts power efficiency anti-misalignment due to the consistent magnetic flux across the entire misalignment range.

The remaining sections of this paper are organized as follows. Section II discusses the challenge of achieving misalignment tolerance with the rectangular-solenoidal pad (RSP) due to zero-crossing polarity reversal. Section III provides a comprehensive design approach to eliminate the need for control in the IPT system using the Tx RSP and Rx rectangular pad (RP). Section IV presents the experimental validation of the proposed method, and Section V concludes the paper.

II. Challenge of Zero-Crossing Polarity Reversal for Achieving Misalignment Tolerance

Fig. 1 illustrates the proposed Tx pad, which integrates a rectangular coil and a solenoidal coil into a single unit known as the rectangular-solenoidal pad (RSP). The solenoidal coil is wound around the magnetic core in an orthogonal layout with the rectangular coil, ensuring magnetic decoupling between them. The rectangular coil generates a vertical magnetic field, while the solenoidal coil produces a parallel magnetic field. On the Rx side, a single rectangular pad (RP) is magnetically coupled with both the solenoidal and rectangular coils on the Tx side. Unless specified otherwise, the subscripts $\mathrm{T1}$, $\mathrm{T2}$, and R are used to denote the associated parameters of the rectangular coil on the Tx side, the solenoidal coil on the Tx side, and the rectangular coil on the Rx side, respectively. For detailed definitions of the geometric parameters, please refer to Table I.

The magnetic connection between the rectangular coil of the transmitter (Tx) and the rectangular coil of the receiver (Rx) is referred to as $\varPhi_{\mathrm{T1R}}$, while the connection between the solenoidal coil of the transmitter (Tx) and the rectangular coil of the receiver (Rx) is referred to as $\varPhi_{\mathrm{T2R}}$. When there is misalignment along the positive or negative X-axis, $\varPhi_{\mathrm{T1R}}$ is always positive because the overall magnetic field passing through the rectangular coil of the receiver (Rx) is positive. However, $\varPhi_{\mathrm{T2R}}$ can have both positive and negative values depending on the direction of misalignment. It becomes negative when there is misalignment along the negative X-axis, and vice versa when there is misalignment along the positive X-axis. According to the Neumann formula, the mutual inductances can be derived as

$$M_{\mathrm{T1R}} = \frac{\varPhi_{\mathrm{T1R}}}{I_{\mathrm{T1}}}, \text{ and} \tag{1}$$

$$M_{\mathrm{T2R}} = \frac{\varPhi_{\mathrm{T2R}}}{I_{\mathrm{T2}}}, \tag{2}$$

where I_{T1} and I_{T2} are the currents that excite the Tx rectangular coil and the Tx solenoidal coil respectively. Thus, M_{T2R} undergoes zero-crossing polarity reversal, which poses challenges to achieve misalignment tolerance.

The mutual inductances versus the X-axis misalignment are calculated through finite element analysis using ANSYS Maxwell, with the geometric parameters of the proposed coupler provided in Table I. The results, depicted in Fig. 2, illustrate the behavior of M_{T1R} and M_{T2R}. M_{T1R} is represented by the markers "–◯–", and it exhibits axial symmetry, gradually decreasing as the offset along the X-axis increases in either direction. Conversely, M_{T2R} displays central symmetry and features a zero-crossing point, denoted by the markers "–◯–".

When examining the right half-plane, M_{T1R} and M_{T2R} exhibit contrasting behaviors, which presents an opportunity for achieving misalignment tolerance. However, in the left half-plane, both M_{T1R} and M_{T2R} decrease as misalignment increases. Without inherent complementary characteristics, additional control efforts would be necessary to achieve misalignment tolerance. For example, by adjusting I_{T2} based on the sign of $\varPhi_{\mathrm{T2R}}$ as stated in (2), the left half-plane trend of M_{T2R} can be mirrored along the X-axis to match the complementary trend of M_{T1R} seen in the right half-plane, as shown in Fig. 2. However, implementing such an active method would involve intricate detection and control processes. This motivates us to develop a fully passive scheme that can achieve misalignment tolerance across the entire X-

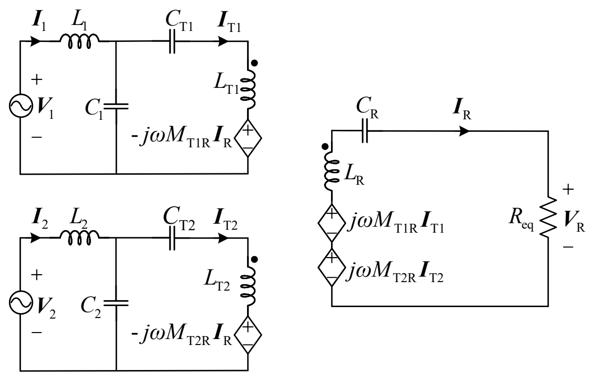

Fig. 4. Equivalent circuit for the system shown in Fig. 3.

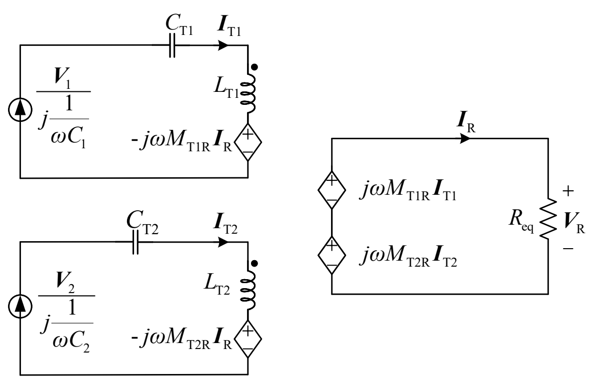

Fig. 5. Simplified version for the circuit shown in Fig. 4.

axis, regardless of the challenges posed by polarity reversal at zero-crossings, as elaborated in the subsequent sections.

III. Design for Eliminating Control Using Tx Rectangular-Solenoid Pad

A. Schematics and Modeling

A control-free and misalignment-tolerant IPT system utilizes the configuration shown in Fig. 3. The system consists of a Tx RSP and an Rx RP, forming a loosely-coupled transformer. The rectangular and solenoidal coils of the RSP are represented by L_{T1} and L_{T2} respectively, while the rectangular coil of the Rx is denoted as L_{R}. The mutual inductances between these coils are denoted as M_{T1T2}, M_{T1R}, and M_{T2R}. It is important to note that due to the orthogonal arrangement of the rectangular and solenoidal coils in the RSP, their cross coupling is expected to be minimal. In other words, the mutual inductance M_{T1T2} can be considered negligible compared to M_{T1R} or M_{T2R}, and can therefore be disregarded. To achieve compensation, both the rectangular and solenoidal coils of the RSP are equipped with LCC circuits, forming two separate resonant tanks. These resonant tanks are driven by fixed-frequency (ω) AC sources generated by two full-bridge inverters. The AC outputs of these inverters, known as v_1 and v_2, exhibit a phase difference θ. In the receiver section, the rectangular coil is series compensated, and the induced AC power is converted to a DC output through a rectifier.

Using a fundamental approximation, the circuit model of the IPT system is shown in Fig. 4, where $\boldsymbol{V}_1$, $\boldsymbol{V}_2$, $\boldsymbol{I}_1$, $\boldsymbol{I}_2$, $\boldsymbol{I}_{\mathrm{T1}}$,

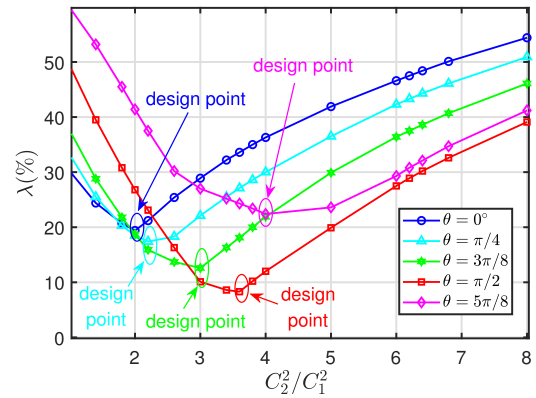

Fig. 6. Fluctuation λ versus C_2^2/C_1^2 under different phase difference θ of excitation currents.

$\boldsymbol{I}_{\mathrm{T2}}$, $\boldsymbol{V}_{\mathrm{R}}$ and $\boldsymbol{I}_{\mathrm{R}}$ are vectors of fundamentals of v_1, v_2, i_1, i_2, i_{T1}, i_{T2}, v_{R} and i_{R} respectively, and $R_{\mathrm{eq}}=\frac{8}{\pi^2}\frac{V_{\mathrm{O}}}{I_{\mathrm{O}}}$ is defined as the equivalent load resistance of the rectifier as well as the load resistance. Since there is a phase difference θ between v_1 and v_2, the relationship between $\boldsymbol{V}_1$ and $\boldsymbol{V}_2$ can be derived as

$$\boldsymbol{V}_2=\boldsymbol{V}_1\angle\theta. \tag{3}$$

When designing the IPT system, some LC circuits are designed to be resonant as expressed by (4), which include L_1–C_1, L_2–C_2 and L_{R}–C_{R}, i.e.,

$$\omega L_1-\frac{1}{\omega C_1}=\omega L_2-\frac{1}{\omega C_2}=\omega L_{\mathrm{R}}-\frac{1}{\omega C_{\mathrm{R}}}=0. \tag{4}$$

Using Thévenin's and Norton's Theorems, the circuit model can be further simplified, as given in Fig. 5. It can be observed that the IPT system is equivalent to being driven by two current sources, i.e.,

$$\boldsymbol{I}_{\mathrm{T1}}=\frac{\boldsymbol{V}_1}{j\frac{1}{\omega C_1}},\ \text{and} \tag{5}$$

$$\boldsymbol{I}_{\mathrm{T2}}=\frac{\boldsymbol{V}_2}{j\frac{1}{\omega C_2}}=\frac{\boldsymbol{V}_1\angle\theta}{j\frac{1}{\omega C_2}}, \tag{6}$$

The circuit equations of the IPT system are given by

$$\begin{aligned}0&=(\frac{1}{j\omega C_{\mathrm{T1}}}+j\omega L_{\mathrm{T1}})\boldsymbol{I}_{\mathrm{T1}}-j\omega M_{\mathrm{T1R}}\boldsymbol{I}_{\mathrm{R}},\\0&=(\frac{1}{j\omega C_{\mathrm{T2}}}+j\omega L_{\mathrm{T2}})\boldsymbol{I}_{\mathrm{T2}}-j\omega M_{\mathrm{T2R}}\boldsymbol{I}_{\mathrm{R}},\\\boldsymbol{V}_{\mathrm{R}}&=R_{\mathrm{eq}}\boldsymbol{I}_{\mathrm{R}}=j\omega M_{\mathrm{T1R}}\boldsymbol{I}_{\mathrm{T1}}+j\omega M_{\mathrm{T2R}}\boldsymbol{I}_{\mathrm{T2}}.\end{aligned} \tag{7}$$

With (7), output voltage $\boldsymbol{V}_{\mathrm{R}}$ is given by

$$\boldsymbol{V}_{\mathrm{R}}=\omega^2C_1M_{\mathrm{T1R}}\boldsymbol{V}_1+\omega^2C_2M_{\mathrm{T2R}}\boldsymbol{V}_1\angle\theta. \tag{8}$$

The amplitude of $\boldsymbol{V}_{\mathrm{R}}$ is given by (9).

$$|\boldsymbol{V}_{\mathrm{R}}|=\omega^2C_1\,|\boldsymbol{V}_1|\,\beta, \tag{9}$$

where

$$\beta=\sqrt{\underbrace{\frac{2C_2M_{\mathrm{T1R}}M_{\mathrm{T2R}}\cos\theta}{C_1}}_{\text{Term }①}+\underbrace{M_{\mathrm{T1R}}^2+\frac{C_2^2}{C_1^2}M_{\mathrm{T2R}}^2}_{\text{Term }②}}. \tag{10}$$

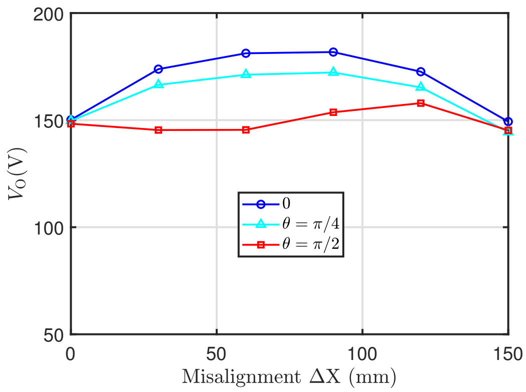

Fig. 7. Output voltage versus misalignment along X-axis under different phase difference θ of excitation currents.

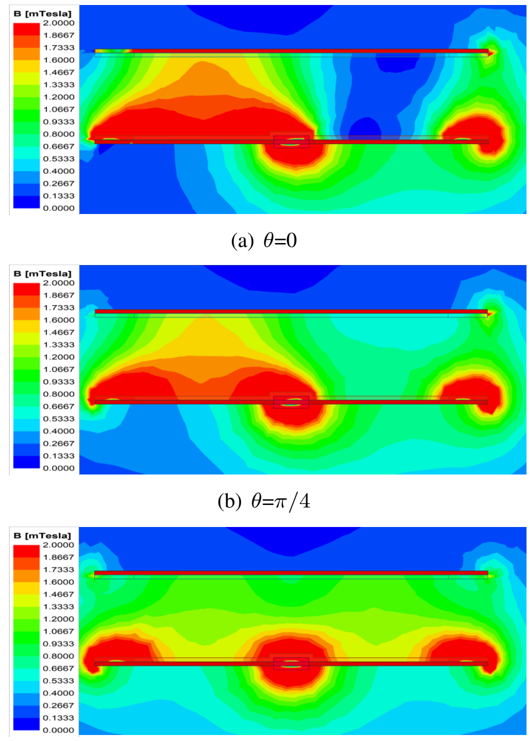

(a) θ=0

(b) $\theta=\pi/4$

(c) $\theta=\pi/2$

Fig. 8. Magnetic flux density of the RSP-RP coupler under different phase difference θ of excitation currents.

One can notice that the output voltage is linked to M_{T1R} and M_{T2R}. However, since there are two distinct terms involved, the fundamental concept to achieve control-free misalignment tolerance can be derived as follows.

1) Term ① is relevant to the polarity of M_{T1R} and M_{T2R}. As illustrated in Section II, M_{T2R} exhibits zero-crossing polarity reversal, causing term ① to encounter the same issue. Polarity detection of M_{T2R} and reverse shifting of θ are commonly-used active way to address this issue. Alternatively, to fully eliminate the control effort, ① can be nullified by setting θ to be $\pi/2$.
2) Term ② is irrelevant to the polarity of M_{T1R} and M_{T2R}. Since the changes of M^2_{T1R} and M^2_{T2R} have opposite trends when there is misalignment, it is possible to make the changes approximately complementary via the design of C_1 and C_2. Thus, a nearly constant ② irrespective of misalignment can be achieved.

After fulfilling the aforementioned criteria for term ① and term ②, the IPT system can attain misalignment tolerance without the need for complicated detection and active control. Additionally, as shown in equation (9), the output voltage remains unaffected by the load and consistently provides a constant voltage output. This can be adjusted by tuning the compensation parameter C_1 and is not constrained by the magnetic coupler.

B. Anti-Misalignment Design and Merits of Control-Free Method

By making term ① zero, i.e., $\theta = \pi/2$, the output DC voltage of the proposed IPT system can be calculated as

$$V_{\mathrm{O}} = \omega^2 V_{\mathrm{DC}} C_1 \sqrt{M^2_{\mathrm{T1R}} + \frac{C_2^2}{C_1^2} M^2_{\mathrm{T2R}}}. \tag{11}$$

The voltage V_{O} remains unaffected by the polarity of the mutual inductance, indicating that the proposed IPT system can function without the need for extra control strategies, detections, or communications.

From (11), the fluctuation of output voltage V_{O} caused by misalignment is determined by a factor Δ given by

$$\Delta = M^2_{\mathrm{T1R}} + \frac{C_2^2}{C_1^2} M^2_{\mathrm{T2R}}. \tag{12}$$

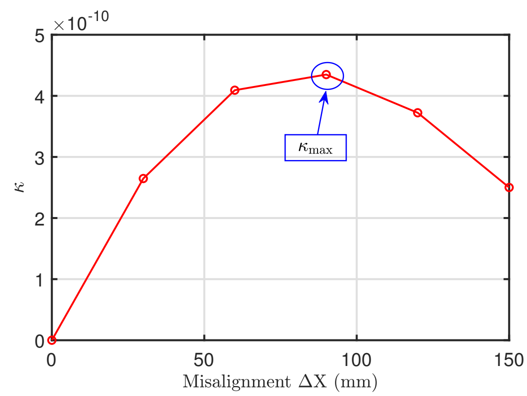

Fig. 9. κ versus misalignment along X-axis (misalignment in the negative direction is symetric).

As shown in (12), mutual inductances M_{T1R}, M_{T2R}, and C_2^2/C_1^2 are factors affecting the fluctuation of the output voltage. Thus, an intuitive method is to adjust M_{T1R} and M_{T2R} based on the parameter design of the magnetic coupler for pad misalignment tolerance. This approach will significantly constrain the design freedom of the coupler and expect to be time-consuming. As plotted in Fig. 2, the absolute value of mutual inductances M_{T1R} and M_{T2R} have opposite trends and in a complementary manner within a wide range of pad misalignment. One can note that by choosing the ratio of C_2^2/C_1^2 appropriately, Δ can be made relatively consistent despite misalignment. This means that the range of variation in output voltage V_{O} can be controlled within a specific limit

$$
\begin{aligned}
Z_{\mathrm{In1}} &= \frac{\boldsymbol{V}_1}{\boldsymbol{I}_1} = \frac{1}{j\left[\frac{\omega^4 C_1 C_2 M_{\mathrm{T1R}} M_{\mathrm{T2R}}}{R_{\mathrm{eq}}} - \omega C_1(1-\omega^2 C_1 L_{\mathrm{T1}} + \frac{C_1}{C_{\mathrm{T1}}})\right] + \frac{\omega^4 C_1^2 M_{\mathrm{T1R}}^2}{R_{\mathrm{eq}}}}, \\
Z_{\mathrm{In2}} &= \frac{\boldsymbol{V}_1}{\boldsymbol{I}_1} = \frac{1}{j\left[\frac{\omega^4 C_1 C_2 M_{\mathrm{T1R}} M_{\mathrm{T2R}}}{R_{\mathrm{eq}}} - \omega C_2(1-\omega^2 C_2 L_{\mathrm{T2}} + \frac{C_2}{C_{\mathrm{T2}}})\right] + \frac{\omega^4 C_2^2 M_{\mathrm{T2R}}^2}{R_{\mathrm{eq}}}}.
\end{aligned}
\tag{14}
$$

$$
\begin{aligned}
\varphi_1 &= \frac{180}{\pi}\arctan\frac{\Im(Z_{\mathrm{In1}})}{\Re(Z_{\mathrm{In1}})} = \frac{180}{\pi}\arctan\left(\frac{\omega C_1(1-\omega^2 C_1 L_{\mathrm{T1}} + \frac{C_1}{C_{\mathrm{T1}}})R_{\mathrm{eq}} - \omega^4 C_1 C_2 M_{\mathrm{T1R}} M_{\mathrm{T2R}}}{\omega^4 C_1^2 M_{\mathrm{T1R}}^2}\right), \\
\varphi_2 &= \frac{180}{\pi}\arctan\frac{\Im(Z_{\mathrm{In2}})}{\Re(Z_{\mathrm{In2}})} = \frac{180}{\pi}\arctan\left(\frac{\omega C_2(1-\omega^2 C_2 L_{\mathrm{T2}} + \frac{C_2}{C_{\mathrm{T2}}})R_{\mathrm{eq}} - \omega^4 C_1 C_2 M_{\mathrm{T1R}} M_{\mathrm{T2R}}}{\omega^4 C_2^2 M_{\mathrm{T2R}}^2}\right).
\end{aligned}
\tag{15}
$$

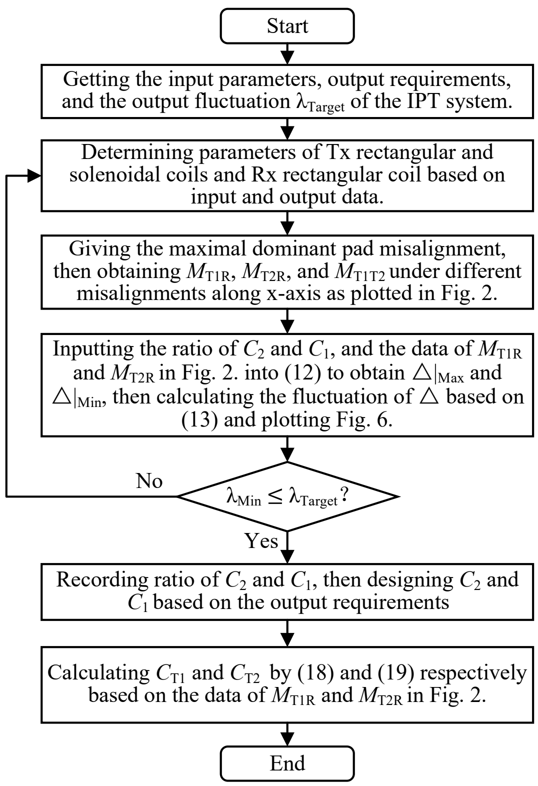

Fig. 10. Design flowchart for the proposed IPT system.

value. The fluctuation of Δ is defined as

$$
\lambda = \frac{\Delta|_{\mathrm{Max}} - \Delta|_{\mathrm{Min}}}{\Delta|_{\mathrm{Max}} + \Delta|_{\mathrm{Min}}} \times 100\%, \tag{13}
$$

where $\Delta|_{\mathrm{Max}}$ and $\Delta|_{\mathrm{Min}}$ are the maximum and minimum values of Δ versus the misalignment along X-axis, respectively.

According to equation (13) and the simulated mutual inductances shown in Fig. 2, the plot in Fig. 6 illustrates the fluctuation value λ versus C_2^2/C_1^2 under different excitation phase difference θ. It can be observed that λ first decreases and then increases with the increase of the ratio of C_2^2/C_1^2. Thus, when λ becomes the minimum value, the corresponding ratio of C_2 and C_1 is the optimal design point for the proposed IPT system to achieve the best misalignment tolerance capability. Notably, the minimum fluctuation value occurs at $\theta = \pi/2$ and is within 10%, significantly smaller than the values at $\theta = 0$, $\theta = \pi/4$, $\theta = 3\pi/8$, and $\theta = 5\pi/8$. Furthermore, Fig. 7 demonstrates the output voltage versus misalignment using the optimal design of C_2^2/C_1^2 for the minimum value of λ across different settings of θ. These results further confirm that $\theta = \pi/2$ significantly reduces output voltage fluctuations due to misalignment. The proposed IPT system with $\theta = \pi/2$ achieves excellent anti-misalignment performance with the optimal design of C_1 and C_2. To analyze the loosely-coupled transformer, FEA analysis is conducted in ANSYS Maxwell with excitation currents having various phase differences (i.e., $\theta = 0$, $\theta = \pi/4$, $\theta = \pi/2$), as shown in Fig. 8. The amplitudes of the excitation currents are set to 10 A. When the phase difference is 0 or $\pi/4$, the magnetic field distribution is asymmetrical, with a significant imbalance between the left and right sides. This imbalance poses a risk of magnetic saturation [33]. However, with a phase difference of $\pi/2$, the magnetic field distribution becomes symmetrical, effectively reducing core loss and the risk of magnetic saturation [34]. Therefore, the proposed polarity-regardless excitation method (i.e., $\theta = \pi/2$) exhibits better magnetic field distribution characteristics between the Tx rectangular and solenoidal coils in the RSP-RP coupler. This advantage further highlights the effectiveness of the proposed excitation method for the control-free IPT system.

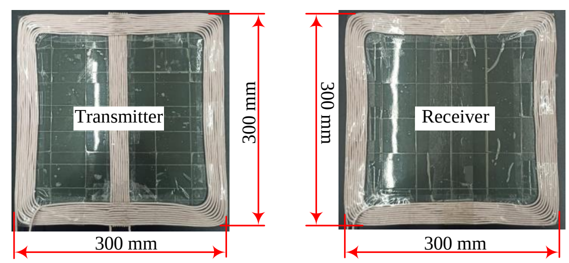

Fig. 11. Proposed RSP-RP coupler.

C. Consideration for Soft Switching

With $\theta = \pi/2$, the input impedances Z_{In1} and Z_{In2} can be determined using equation (14). Based on equation (14), the input phase angles can be obtained through equation (15), where $\Im$ and $\Re$ correspond to the imaginary and real components of the respective impedance. According to (15),

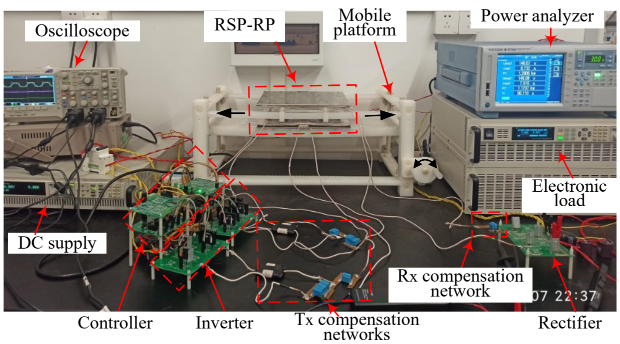

Fig. 12. Experimental prototype of 1-kW proposed control-free IPT system.

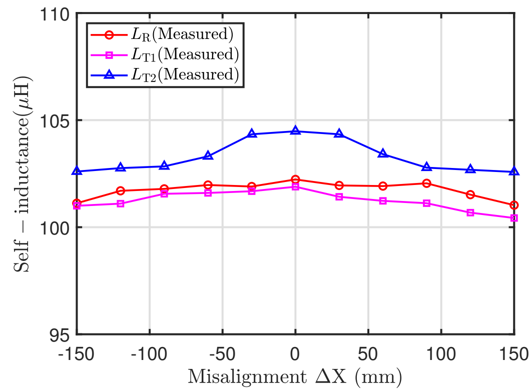

Fig. 13. Measured self-inductances versus misalignment along X-axis.

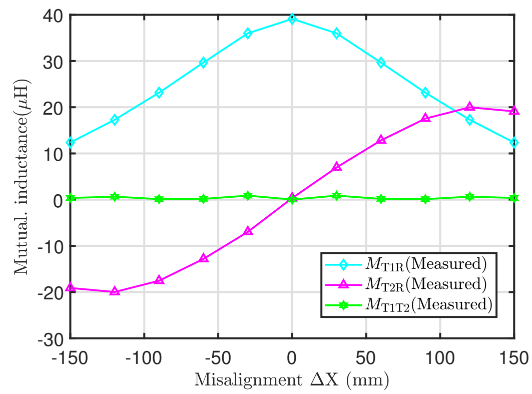

Fig. 14. Measured mutual inductances versus misalignment along X-axis.

the input phase angles φ_1 and φ_2 should be maintained positive for zero voltage switching (ZVS) by appropriately designing the compensation capacitors C_{T1} and C_{T2}. Thus, the design boundaries of compensation capacitors C_{T1} and C_{T2} are given by

$$C_{T1} \leq \frac{C_1}{\frac{\omega^3 C_2 |M_{T1R}||M_{T2R}|}{R_{eq}} + \omega^2 C_1 L_{T1} - 1}, \text{ and} \quad (16)$$

$$C_{T2} \leq \frac{C_2}{\frac{\omega^3 C_1 |M_{T1R}||M_{T2R}|}{R_{eq}} + \omega^2 C_2 L_{T2} - 1}, \quad (17)$$

respectively. It can be observed that the design of C_{T1} and C_{T2} is influenced by the term $\kappa = |M_{T1R}||M_{T2R}|$. To achieve ZVS throughout the whole misalignment range, the maximum κ, i.e., κ_{max}, should be considered. With the mutual inductances shown in Fig. 2, κ over the whole misalignment range can be calculated, as plotted in Fig. 9. With κ_{max} obtained in the figure, the design criteria for C_{T1} and C_{T2} are given by

$$C_{T1} \leq \frac{C_1}{\frac{\omega^3 C_2 \kappa_{max}}{R_{eq}} + \omega^2 C_1 L_{T1} - 1}, \quad (18)$$

$$C_{T2} \leq \frac{C_2}{\frac{\omega^3 C_1 \kappa_{max}}{R_{eq}} + \omega^2 C_2 L_{T2} - 1}, \quad (19)$$

respectively.

Given the aforementioned analysis, a design flowchart to detail the design procedure and consideration for the proposed IPT system is shown in Fig. 10. The design procedure of the proposed system can be summarized as follows.

1) We first get the input parameters (eg., input DC voltage, input power, operating frequency, etc.), the output requirements (eg., output voltage, output current or output rated power, etc.), and output fluctuation λ_{Target} of the proposed IPT system. Then, we determine the parameters of the Tx rectangular and solenoidal coils, and the Rx rectangular coil according to the input and output data.
2) We set the maximal dominant pad misalignment and obtain the mutual inductances (M_{T1R}, M_{T2R}, and M_{T1T2}) between the Tx rectangular coil and Rx rectangular coil, Tx solenoidal coil and Rx rectangular coil, and Tx rectangular coil and Tx solenoidal coil respectively under different misalignments, as plotted in Fig. 2. Then, we substitute the ratio of C_2 and C_1, as well as the data of M_{T1R} and M_{T2R} in Fig. 2 into equation (12) to obtain $\Delta|_{Max}$ and $\Delta|_{Min}$. Then, we put $\Delta|_{Max}$ and $\Delta|_{Min}$ into equation (13) to calculate the fluctuation of Δ and plot Fig. 6. When the fluctuation $\lambda_{Min} \leq \lambda_{Target}$, the corresponding ratio value of C_2 and C_1 is the optimal design point for the proposed IPT system to achieve the best misalignment tolerance capability. Thus, we record this ratio of C_2 and C_1 and design C_2 and C_1 based on the output requirements. On the other hand, if $\lambda_{Min} \geq \lambda_{Target}$, turns number N_{T2} of the Tx solenoidal coil should be reselected, and then redesign the IPT system according to the above process.
3) Finally, we calculate C_{T1} and C_{T2} by equations (18) and (19) respectively based on the data of M_{T1R} and M_{T2R} in Fig. 2.

IV. Experimental Verification

A. Experiment Setup

Based on the geometric specifications given in Table I, a magnetic coupler is constructed, comprising a Tx RSP and a Rx RP. The photos of these two pads are shown in Fig. 11. An LCR meter (model: HIOKI IM3536) is used to measure the magnetic coupler and the parameters are summarized in Table II. According to the circuit diagram of the proposed IPT system in Fig. 3, a 1-kW experimental prototype is built as shown in Fig. 12. The two inverters share

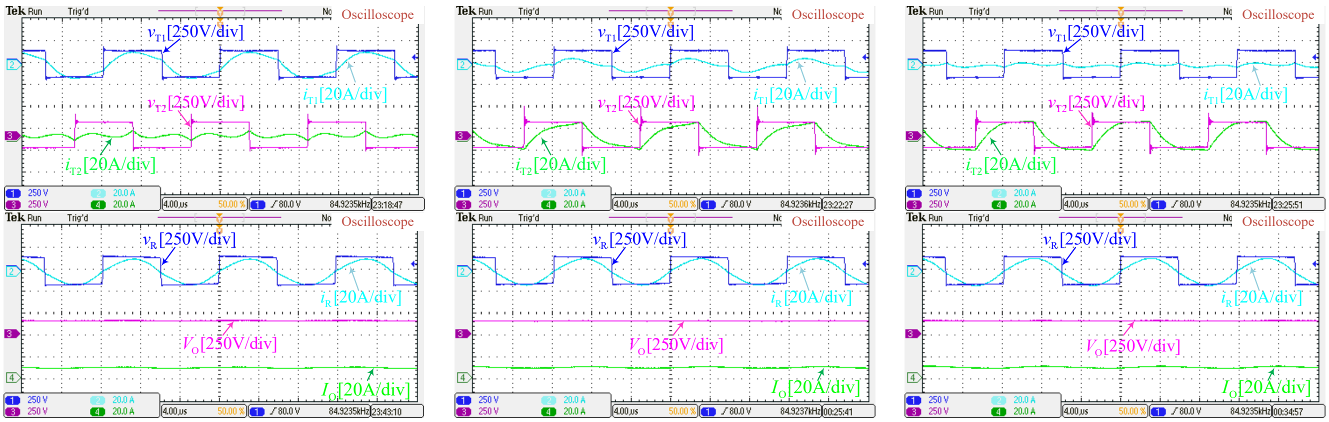

(a) ΔX = 0 mm (fully aligned) (b) ΔX = 75 mm (ΔX = -75 mm) (c) ΔX = 150 mm (ΔX = -150 mm)

Fig. 15. Experimental waveforms of the proposed control-free IPT system at various misalignment conditions.

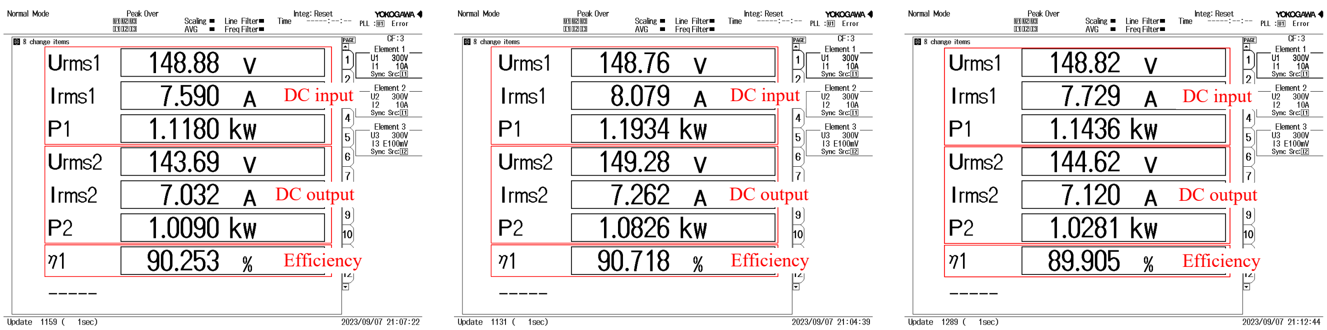

(a) ΔX=-150 mm (b) ΔX=0 mm (fully aligned) (c) ΔX=150 mm

Fig. 16. Captured power analysis at various misalignment conditions.

a digital controller. The controller generates two groups of PWM signals to drive the two independent inverters. The phase difference between these two group PWMs is set to be 90°, such that it can achieve a phase difference of 90° between the two independent inverters. The circuit parameters are summarized in Table II. There is no device used for complex detection and active control. A programmable DC electronic load (model: DH27605B) is used to emulate the load and a power analyzer (Model: YOKOGAWA WT1803E) is used to measure the power efficiency. To simulate the misalignment scenario relevant to electric vehicles, an ABS-made mobile platform simulating a vehicle chassis is employed.

TABLE II
MEASURED PARAMETERS OF THE IPT PROTOTYPE

	Parameters	Symbols	Values
	Self inductance of Tx RP (fully aligned)	L_{T1}	101.9 μH
	Self inductance of Tx SP (fully aligned)	L_{T2}	104.5 μH
	Self inductance of Rx RP (fully aligned)	L_R	102.2 μH
Circuit Parameters	Parameters	Symbols	Values
	Input voltage	V_{DC}	150 V
	Compensation capacitor	C_1, C_{T1}	88.6 nF, 45.6 nF
		C_2, C_{T2}	168.1 nF, 40.1 nF
		C_R	34.4 nF
	Compensation inductor	L_1, L_2	39.57 μH, 20.86 μH
	Filter	C_{f1}	1.0 mF
	Load resistance	R_L	20.5 Ω
	Diodes	D_1-D_4	MBR20200CTG
	MOSFETs	Q_1-Q_8	STC4050
	Operating frequency	f	85 kHz

B. Measured Parameters of Magnetic Coupler Against Misalignment

Fig. 13 shows the measured self-inductances (L_{T1}, L_{T2}, and L_R) versus the X-axis misalignment and the variation of the self-inductances is within 1.8%, allowing them to be treated as constant in the design of compensation parameters. Fig. 14 shows the measured mutual inductances versus the X-axis misalignment, where M_{T1R} is axially symmetric and it decreases with the increase of offset along either direction of the X-axis, while M_{T2R} exhibits central symmetry with a zero-crossing point, which is consistent with the analysis in Section II. Besides, M_{T1T2} is approximately zero and significantly smaller than M_{T1R} or M_{T2R}. Thus, the solenoidal coil and rectangular coil on the Tx side are magnetically decoupled.

C. Measured Output

The operational waveforms under full load conditions are displayed in Fig. 15. Three scenarios of misalignment are examined, with X-axis displacements of $\Delta X = 0, 75, 150$ mm. The misalignment range spans from -150 mm to +150 mm, equivalent to about 50% of the proposed RSP length. It is evident that a consistent phase lag of 90° exists between

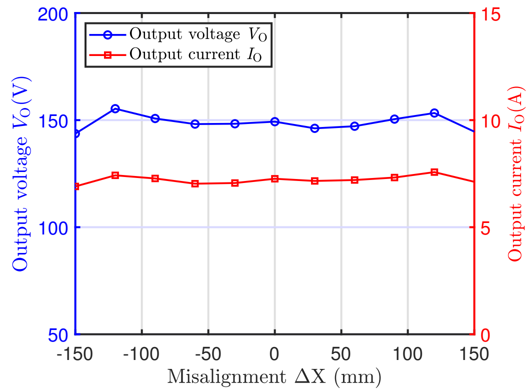

Fig. 17. Measured output voltage and current versus misalignment along X-axis.

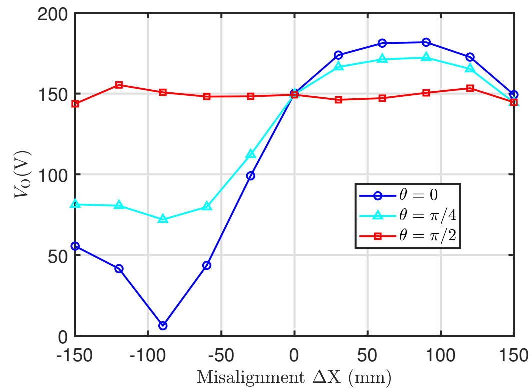

Fig. 19. Output voltage versus X-misalignment for different values of excitation phase difference θ.

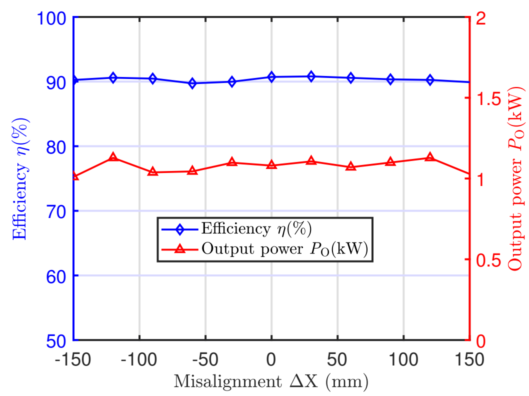

Fig. 18. Measured DC-to-DC efficiency versus misalignment along X-axis.

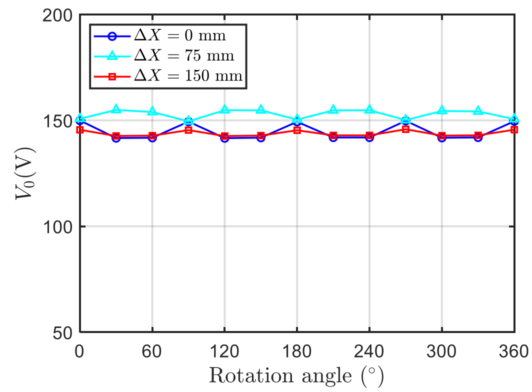

Fig. 20. Output voltage of the proposed IPT system at different X-misalignment conditions during the rotational movement of the receiver.

the modulated voltages V_{T2} and V_{T1}. Additionally, under all misalignment conditions, i_{T1} and i_{T2} lag behind V_{T1} and V_{T2} respectively, indicating the potential for achieving zero voltage switching (ZVS) in the inverters. The output voltage hovers around 150 V, as shown in Fig. 17. As the X-axis misalignment varies from -150 mm to +150 mm, the voltage fluctuates between 143.7 V and 155.3 V. This fluctuation, which remains within 4% over a misalignment of 50% of the RSP length, demonstrates a resilient tolerance towards misalignment. The captured efficiencies at $\Delta X = -150,\ 0,\ 150$ mm are shown in Fig. 16, and detailed efficiency versus misalignment are plotted in Fig. 18. The efficiency ranges from 90.718% to 89.905% over a misalignment of 50% of the RSP length and the fluctuation is within 0.8%. The efficiency remains almost constant and there is no significant efficiency degradation as the increase of misalignment. The misalignment-insensitive efficiency performance stands as another advantage of the proposed scheme.

The output voltage of the proposed IPT system under different X-misalignment conditions with different excitation phase difference θ is shown in Fig. 19. As illustrated in Fig. 19, the fluctuation of the output voltage is significant in the proposed system with the excitation phase difference configurated at $\theta = 0$ and $\theta = \pi/4$. However, the proposed system can achieve excellent anti-misalignment performance with $\theta = \pi/2$. In addition, Fig. 20 shows the output voltage V_O at different X-misalignment conditions (i.e., ΔX = 0 mm, ΔX = 75 mm, and ΔX = 150 mm) during the rotational movement of the receiver. It can be observed that the output voltages V_O of the proposed IPT system can also achieve excellent stable capability under different rotation conditions.

Fig. 21 illustrates the power loss breakdown for the proposed IPT system under different X-misalignment conditions. It can observed that when the receiver is fully aligned with the Tx pad (i.e., ΔX= 0 mm), the total power loss is P_{Loss} = 110.8 W, as illustrated in Fig. 21(a). For ΔX = 150 mm, the total power loss is P_{Loss} = 115.5 W, as shown in Fig. 21(b). Furthermore, the loosely coupled transformer (RSP + RP) consumes the highest power of all the components. Thus, the system efficiency can be improved by adopting better winding materials with low resistivity and magnetic materials, along with an optimized design of the ferrite.

V. Conclusion

This paper presents a novel inductive power transfer (IPT) system that can tolerate misalignment. The system utilizes a hybrid transmitter (Tx) pad with rectangular and solenoidal coils, along with a receiver pad equipped with a rectangular coil. The proposed design effectively counteracts misalignment issues, allowing the system to maintain a constant voltage output without the need for additional control, detection, or

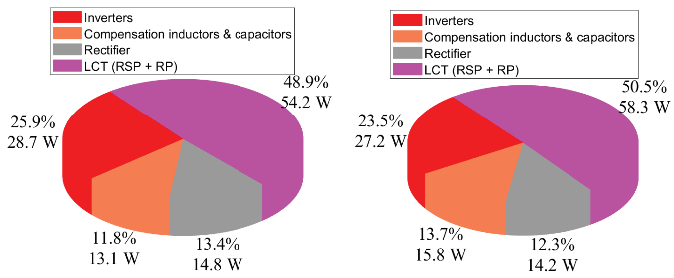

(a) $\Delta X = 0$ mm (b) $\Delta X = 150$ mm

Fig. 21. Power loss breakdown at full load of the proposed IPT system under different pad misalignment conditions

communication mechanisms. Furthermore, the system demonstrates remarkable efficiency in the face of misalignment, with a power efficiency of approximately 90% even when the misalignment ranges from −50% to 50% of the Tx pad length. The paper also provides a comprehensive overview of the system structure, detailed modeling, and theoretical analysis. Emphasis is placed on minimizing output fluctuations and ensuring smooth switching, which greatly facilitates parameter design for practical applications.

REFERENCES

[1] X. Qu, W. Zhang, S. C. Wong, and C. K. Tse, "Design of a current-source-output inductive power transfer led lighting system," *IEEE J. Emerg. Sel. Topics Power Electron.*, vol. 3, no. 1, pp. 306–314, Mar. 2015.

[2] Y. Zeng, C. Rong, C. Lu, X. Tao, X. Liu, R. Liu, and M. Liu, "Misalignment insensitive wireless power transfer system using a hybrid transmitter for autonomous underwater vehicles," *IEEE Trans. Ind. Appl.*, vol. 58, no. 1, pp. 1298–1306, Feb. 2022.

[3] Q. Wang, W. Che, M. Mongiardo, and G. Monti, "Wireless power transfer system with high misalignment tolerance for bio-medical implants," *IEEE Trans. Circuits Syst. II, Exp. Briefs*, vol. 67, no. 12, pp. 3023–3027, Dec. 2020.

[4] D. Wang, X. Qu, Y. Yao, and P. Yang, "Hybrid inductive-power-transfer battery chargers for electric vehicle onboard charging with configurable charging profile," *IEEE Trans. Intell. Transp. Syst.*, vol. 22, no. 1, pp. 592–599, Jan. 2021.

[5] W. Zhang, J. C. White, A. M. Abraham, and C. C. Mi, "Loosely coupled transformer structure and interoperability study for EV wireless charging systems," *IEEE Trans. Power Electron.*, vol. 30, no. 11, pp. 6356–6367, Nov. 2015.

[6] M. Moghaddami and A. Sarwat, "Self-tuning variable frequency controller for inductive electric vehicle charging with multiple power levels," *IEEE Trans. Transport. Electrific.*, vol. 3, no. 2, pp. 488–495, Jun. 2017.

[7] K. Song, G. Yang, Y. Guo, Y. Lan, S. Dong, J. Jiang, and C. Zhu, "Design of DD coil with high misalignment tolerance and low emf emissions for wireless electric vehicle charging systems," *IEEE Trans. Power Electron.*, vol. 35, no. 9, pp. 9034–9045, Sep. 2020.

[8] S. Bandyopadhyay, P. Venugopal, J. Dong, and P. Bauer, "Comparison of magnetic couplers for IPT-based EV charging using multi-objective optimization," *IEEE Trans. Veh. Technol.*, vol. 68, no. 6, pp. 5416–5429, Jun. 2019.

[9] SAE Standard, "Wireless power transfer for light-duty plug-in electric vehicles and alignment methodology," *SAE J2954 TIR*, 2017.

[10] S. Kim, G. A. Covic, and J. T. Boys, "Comparison of tripolar and circular pads for ipt charging systems," *IEEE Trans. Ind. Electron.*, vol. 33, no. 7, pp. 6093–6103, Jul. 2018.

[11] S. Kim, G. A. Covic, and J. T. Boys, "Tripolar pad for inductive power transfer systems for ev charging," *IEEE Trans. Ind. Electron.*, vol. 32, no. 7, pp. 5045–5057, Jul. 2017.

[12] S. A. Al Mahmud, I. Panhwar, and P. Jayathurathnage, "Large-area free-positioning wireless power transfer to movable receivers," *IEEE Trans. Ind. Electron.*, vol. 69, no. 12, pp. 12807–12816, Dec. 2022.

[13] P. Jayathurathnage, Y. Liu, and J. Kyyra, "Self-decoupled and integrated coils for modular multitransmitter wireless power transfer systems," *IEEE Trans. Power Electron.*, vol. 37, no. 11, pp. 12962–12967, Nov. 2022.

[14] L. Zhao, D. J. Thrimawithana, and U. K. Madawala, "Hybrid bidirectional wireless EV charging system tolerant to pad misalignment," *IEEE Trans. Ind. Electron.*, vol. 64, no. 9, pp. 7079–7086, Sep. 2017.

[15] L. Zhao, D. J. Thrimawithana, U. K. Madawala, A. P. Hu, and C. C. Mi, "A misalignment-tolerant series-hybrid wireless EV charging system with integrated magnetics," *IEEE Trans. Power Electron.*, vol. 34, no. 2, pp. 1276–1285, Feb. 2019.

[16] G. Ke, Q. Chen, L. Xu, X. Ren, and Z. Zhang, "Analysis and optimization of a double-sided S-LCC hybrid converter for high misalignment tolerance," *IEEE Trans. Ind. Electron.*, vol. 68, no. 6, pp. 4870–4881, Jun. 2021.

[17] X. Qu, Y. Yao, D. Wang, S. C. Wong, and C. K. Tse, "A family of hybrid IPT topologies with near load-independent output and high tolerance to pad misalignment," *IEEE Trans. Power Electron.*, vol. 35, no. 7, pp. 6867–6877, Jul. 2020.

[18] Y. Chen, B. Yang, Z. Kou, Z. He, G. Cao, and R. Mai, "Hybrid and reconfigurable IPT systems with high-misalignment tolerance for constant-current and constant-voltage battery charging," *IEEE Trans. Power Electron.*, vol. 33, no. 10, pp. 8259–8269, Oct. 2018.

[19] H. Feng, T. Cai, S. Duan, X. Zhang, H. Hu, and J. Niu, "A Dual-Side-Detuned Series–Series Compensated Resonant Converter for Wide Charging Region in a Wireless Power Transfer System," *IEEE Trans. Ind. Electron.*, vol. 65, no. 3, pp. 2177-2188, Mar. 2018.

[20] B. Yang, B. Zhang, Z. Zhang, Y. Luo, R. Mai, Z. He, and Y. Chen, "A Clamped IPT System With Adaptive Mode Switching Against Large Coupling Variations," *IEEE Trans. Power Electron.*, vol. 38, no. 9, pp. 11694-11704, Sep. 2023.

[21] J. Mai, Y. Wang, Y. Yao, M. Sun, and D. Xu, "High-misalignment-tolerant IPT systems with solenoid and double D pads," *IEEE Trans. Ind. Electron.*, vol. 69, no. 4, pp. 3527–3535, Apr. 2022.

[22] W. Zhao, X. Qu, J. Lian, and C. K. Tse, "A family of hybrid IPT couplers with high tolerance to pad misalignment," *IEEE Trans. Power Electron.*, vol. 37, no. 3, pp. 3617–3625, Mar. 2022.

[23] Y. Chen, R. Mai, Y. Zhang, M. Li, and Z. He, "Improving misalignment tolerance for IPT system using a third-coil," *IEEE Trans. Power Electron.*, vol. 34, no. 4, pp. 3009–3013, Apr. 2019.

[24] P. Zhang, M. Saeedifard, O. C. Onar, Q. Yang, and C. Cai, "A field enhancement integration design featuring misalignment tolerance for wireless EV charging using LCL topology," *IEEE Trans. Power Electron.*, vol. 36, no. 4, pp. 3852–3867, Apr. 2021.

[25] Z. Yuan, M. Saeedifard, C. Cai, Q. Yang, P. Zhang, and H. Lin, "A misalignment tolerant design for a dual-coupled LCC-S-compensated WPT system with load-independent CC output," *IEEE Trans. Power Electron.*, vol. 37, no. 6, pp. 7480–7492, Jun. 2022.

[26] M. Budhia, J. T. Boys, G. A. Covic, and C. Y. Huang, "Development of a single-sided flux magnetic coupler for electric vehicle IPT charging systems," *IEEE Trans. Ind. Electron.*, vol. 60, no. 1, pp. 318–328, Jan. 2013.

[27] A. Zaheer, H. Hao, G. A. Covic, and D. Kacprzak, "Investigation of multiple decoupled coil primary pad topologies in lumped IPT systems for interoperable electric vehicle charging," *IEEE Trans. Power Electron.*, vol. 30, no. 4, pp. 1937–1955, Apr. 2015.

[28] H. Xu, Z. Huang, X. L. Li, and C. K. Tse, "Misalignment-tolerant ipt coupler with enhanced magnetic flux variation suppression and reduced copper usage," *IEEE Trans. on Power Electron.*, vol. 39, no. 8, pp. 10506-10517, Aug. 2024.

[29] S. A. A. Mahmud, Y. Liu, N. Ha-Van, P. Jayathurathnage, and S. A. Tretyakov, "Planar free-positioning wireless power transfer system for industrial and automotive robotic applications," *IEEE Open J. Ind. Electron. Soc.*, Accepted, doi: 10.1109/OJIES.2025.3530527.

[30] N. P. C. Hanspeter Widmer, and L. Sieber, "Wireless power antenna alignment adjustment system for vehicles," U.S. Patent US20110254503A1, 2011.

[31] W. Zhang, J. C. White, A. M. Abraham, and C. C. Mi, "Loosely coupled transformer structure and interoperability study for ev wireless charging systems," *IEEE Trans. Power Electron.*, vol. 30, no. 11, pp. 6356–6367, Nov. 2015.

[32] H. Jo, J. A. Lee, D. H. Sim, W. J. Son, and B. K. Lee, "Magnetic characteristics-based selective driving algorithm of IPT EV systems with DDQ power pad for high-efficiency operation and wide misalignment tolerance," in *Proc. IEEE 11th Int. Conf. Power Electron. ECCE Asia*, May 2023, pp. 1031–1037.

[33] M. Mohammad, S. Choi, Z. Islam, S. Kwak, and J. Baek, "Core design and optimization for better misalignment tolerance and higher range of wireless charging of PHEV," *IEEE Trans. Transport. Electrific.*, vol. 3, no. 2, pp. 445–453, Jun. 2017.

[34] M. Mohammad, S. Choi, and M. E. Elbuluk, "Loss minimization design of ferrite core in a DD-coil-based high-power wireless charging system for electrical vehicle application," *IEEE Trans. Transport. Electrific.*, vol. 5, no. 4, pp. 957–967, Dec. 2019.

Hai Xu received the M.S. degree in agricultural engineering from South China Agricultural University, Guangzhou, China, in 2019 and the Ph.D. degree in power electronics from South China University of Technology, Guangzhou, China, in 2024.

His research interests include wireless power transfer, magnetic coupler design, magnetic modeling, and electric vehicle charging.

Zhicong Huang (Senior Member, IEEE) received the B.Eng. degree in electrical engineering and automation and the M.Eng. degree in mechanical and electronic engineering from the Huazhong University of Science and Technology, Wuhan, China, in 2010 and 2013, respectively, and the Ph.D. degree in power electronics from The Hong Kong Polytechnic University, Hong Kong, in 2018.

In 2019, he was a Postdoctoral Fellow under the UM Macao Talent Program with the State Key Laboratory of Analog and Mixed-Signal VLSI, Macau, China. Since 2020, he has been an Associate Professor with the Shien-Ming Wu School of Intelligent Engineering, South China University of Technology, Guangzhou, China. His research interests include wireless power transfer, artificial intelligence in power electronics, and wave energy converters.

Dr. Huang received the Outstanding Reviewer Award for IEEE Transactions on Power Electronics in 2021 and 2024, the Star Reviewer Award for IEEE Journal on Emerging and Selected Topics in Power Electronics in 2023, and the Best Reviewer for IEEE Journal on Emerging and Selected Topics in Circuits and Systems in 2023. He servers as an Associate Editor for IEEE Transactions on Consumer Electronics.

Xiaolu Lucia Li (Member, IEEE) received the B.Eng. and M.Phil. degrees in electrical engineering from Harbin Institute of Technology, China, in 2014 and 2016, respectively, and the Ph.D. degree in power electronics from Hong Kong Polytechnic University, Hong Kong, in 2019. She is currently an Associate Professor of Integrated Circuits at Sun Yat-sen University, China. Prior to joining Sun Yat-sen University in November 2024, she was a Consultant with the Smart City Division, Hong Kong Productivity Council, and was a Postdoctoral Fellow with the Department of Electrical Engineering, City University of Hong Kong. Her research interests include multiport converters and wireless power transfer.

Chi K. Tse (M'90–SM'97–F'06) received the BEng (Hons) degree with first class honors in electrical engineering and the PhD degree from the University of Melbourne, Australia, in 1987 and 1991, respectively.

He is presently Associate Vice President (Innovation), Director of the Academy of Innovation, and Chair Professor of Electrical Engineering at City University of Hong Kong, Hong Kong. His research interests include power electronics, nonlinear systems and complex network applications.

He was the recipient of a number of research and invention prizes including the IEEE CASS Charles A. Desoer Technical Achievement Award in 2022 and a few Best Paper Prizes from IEEE and other journals, as well as a Grand Prize and Gold Medal in Silicon Valley International Invention Festival 2019. He has been appointed to honorary professorship and distinguished fellowship by a few Australian, Canadian and Chinese universities, including the Chang Jiang Scholar Chair Professor with Huazhong University of Science and Technology, Honorary Professor of Melbourne University, and Distinguished Professor-at-Large with the University of Western Australia. He also served as panel member of Hong Kong Research Grants Council, and member of several professional and government committees.

In 2005, 2010 and 2018, he was selected as an IEEE Distinguished Lecturer. In 2006 he chaired the IEEE CAS Technical Committee on Nonlinear Circuits and Systems. He serves and has served as Editor-in-Chief of IEEE TRANSACTIONS ON CIRCUITS AND SYSTEMS II (2016-2019), IEEE Circuits and Systems Magazine (2013-2016), IEICE Nonlinear Theory and Applications (since 2013); as associate editor of a few other IEEE journals; and on the Editorial Board of IEEE Proceedings (2021-2022). He has served on a number of IEEE committees including the IEEE Fellows Committee and the IEEE Awards Committee, and chaired the Steering Committee for IEEE Transactions on Network Science and Engineering.